Proceedings of the 10th International Conference on Civil Structural and Transportation Engineering (ICCSTE 2025)
July, 2025 | Imperial College London Conference Center, London, United Kingdom
Paper No. 317
DOI: 10.11159/iccste25.317

Experimental Study on Shear Performance of Poplar LVL Beams with Opening in Bending-Shear Region

Anlian Wang[1], Yan Liu[1], Ashraf Ashour[2]
[1] College of Civil Science and Engineering
Yangzhou University, Yangzhou, China
First. dx120230106@stu.yzu.edu.cn; Second. liuyan@yzu.edu.cn
[2] Faculty of Engineering and Digital Technologies
University of Bradford, Bradford, United Kingdom
Third. A.F.Ashour@bradford.ac.uk

Abstract **-** To investigate the shear performance of Italian poplar laminated veneer lumber (LVL) beams with opening in the bending-shear region, six standard specimens were designed and tested under four-point bending. The shear failure mechanisms of the LVL beams with opening under various parameters were analyzed. The results show that the unperforated beam experiences bending failure due to tensile cracking at the mid-span. In contrast, beams with circular opening experience longitudinal shear failure at the ends due to stress concentration around the opening perimeter. The maximum transverse tensile strain around the opening perimeter forms an angle of approximately 45° or 225° relative to the longitudinal axis of beam, consistent with the crack initiation angle. As the diameter-to-height ratio increases to 0.5, both cracking and ultimate load capacities of the beams with circular opening significantly decrease, exhibiting more brittle shear failure. When the diameter-to-height ratio increases from 0.3 to 0.4 and 0. 5, the ratio of cracking to ultimate load capacity increases from 0.79 to 0.80 and 0.81, respectively. Using carbon fiber reinforced polymer (CFRP) wrapping around the openings effectively suppresses crack propagation and enhance the structural performance of the perforated beams. For the beam with a diameter-to-height ratio of 0.4, the ultimately load decreases by 17.9% and 5.22%, respectively, for one and two layers of CFRP wrapping, compared to the unperforated beam.

Keywords**:** LVL beam with opening; CFRP; static test; shear performance

1. Introduction

Laminated Veneer Lumber (LVL) is an engineered wood product manufactured by bonding rotary-cut veneers with water-resistant structural adhesives under heat and pressure, aligning the grain direction of the veneers. Compared to natural timber, LVL significantly enhances mechanical properties by reorganizing the wood to eliminate or disperse material defects [1]. Fast-growing poplar is widely cultivated in China due to its rapid growth and adaptability. However, its low density and soft texture [2] limit its direct application in building structures. Applying LVL technology to fast-growing poplar can effectively improve its material properties, thereby enhancing economic and ecological benefits [1].

In modern timber structures, poplar LVL is commonly used for components such as floor joists or beams. To reduce structural self-weight, lower floor heights, and facilitate pipeline installation, openings are often created in the bending-shear regions of beams or joists. However, these openings significantly compromise the structural integrity of the timber beams, altering stress distribution and inducing stress concentration and crack propagation around the openings [3-6]. Existing research has primarily focused on the effects of openings on the mechanical performance, stress distribution, and failure mechanisms of timber beams. Solid beams under load display uniform stress distribution and progressive bending failure with gradual crack propagation, whereas perforated beams experience rapid crack growth due to localized stress concentration around openings, lacking warning signs of impending failure [5-6]. Once cracks initiate, the load-bearing capacity sharply declines.

Fiber-reinforced polymer (FRP) composites, known for their lightweight, durability, and minimal additional load, have become widely used for timber structure reinforcement [7]. However, existing research [9-11] predominantly focuses on reinforced solid beams, with limited consideration of the impact of openings on structural capacity. Since LVL is an anisotropic material with weak shear and transverse tensile properties, openings can easily induce longitudinal crack

propagation, drastically reducing beam capacity. Therefore, investigating the failure mechanisms of perforated LVL beams and the effects of reinforcement on their mechanical performance is of critical importance.

In this study, six standard specimens of fast-growing poplar LVL beams with openings in bending-shear regions were designed and subjected to four-point bending tests. The effects of diameter-to-height ratios and the number of circumferential CFRP fabric layers around the openings on the shear failure mechanisms were comparatively analyzed.

2. Material and methods

2.1. Materials

The logs used in the tests were sourced from fast-growing plantations in northern Jiangsu Province, China, with the tree species being Populus euramericana (commonly known as "Italian poplar"). The laminated veneer lumber (LVL) produced from this material is referred to as "Italian poplar LVL." The veneers of the Italian poplar LVL had a thickness of 1.90 mm, an average moisture content of 9.12%, and an average density of 528 kg/m³. Table 1 lists the measured average values for the mechanical properties and fracture toughness of poplar LVL. Where, $f_{c,X}$ and $f_{c,Y}$ represent the compressive strength along the X- and Y-axes; $f_{t,X}$ and $f_{t,Y}$ denote the tensile strength along the X- and Y-axes, respectively; $f_{m,Z}$ refers to the bending strength around the Z-axis; for YX the first letter indicates the direction of the normal to the crack plane, while the second letter represents the direction of crack propagation.

Table 1: Mechanical properties and fracture toughness of poplar LVL.

Compressive strength /MPa		Tensile strength /MPa		Bending strength /MPa	Bending elastic modulus /GPa	Fracture toughness/(MPa·mm$^{1/2}$)	
$f_{c,X}$	$f_{c,Y}$	$f_{t,X}$	$f_{t,Y}$	$f_{m,Z}$	Around Z-axis	Mode-I$_{(YX)}$	Mode-II$_{(YX)}$
39.3	4.1	59.3	2.1	67.7	8.41	12.7	154.2

The CFRP sheets have a single-layer thickness of 0.167 mm and a unit area weight of 300 g/m². The measured average longitudinal tensile strength was 3450 MPa, the average modulus of elasticity was 240 GPa, and the average elongation at rapture was 1.6%. The average in-plane shear strength and shear modulus of CFRP along the fiber direction being 47.8 MPa and 5.7 GPa, respectively.The mechanical properties of bonding adhesive have been measured. The tensile strength is 54.5 MPa, the compressive strength is 100.7 MPa, and the flexural strength is 76.3 MPa. The tensile modulus is 3.3 GPa, and the elongation at break is 2.1%.

2.2. Specimen design and fabrication

Six beams with holes in the bending-shear span were designed and fabricated, all with dimensions of 100 mm × 300 mm × 3300 mm (width × height × length). The specifications and dimensions of the specimens are shown in Figure 1. "S-0.4-2C" indicates that "0.4" represents the diameter-to-height ratio, and "2C" denotes the application of two layers of CFRP wrapping in the circumferential direction. Table 2 presents the specific design schemes for all specimens.

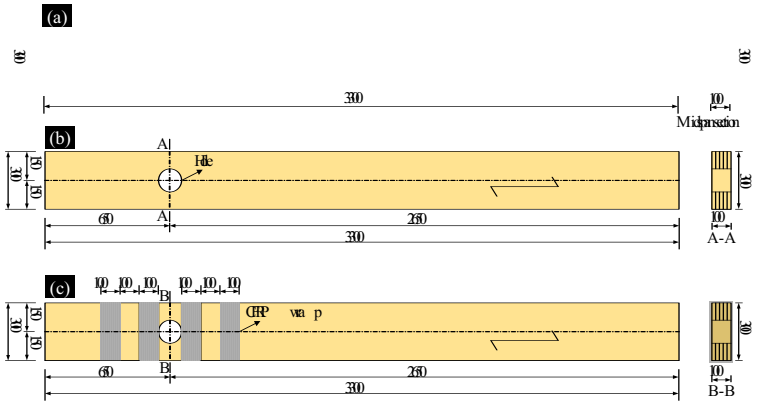

Fig. 1: Configuration of LVL beams (unit: mm): (a) S-0; (b) S-0.3, S-0.4 and S-0.5; (c) S-0.4-1C and S-0.4-2C.

Table 2: Details of specimens.

No.	Hole diameter /mm	Diameter-to-height ratio	Number of CFRP layer	Test objective
S-0	0	0	0	Beam without hole, control Specimen
S-0.3	90	0.3	0	Analyzing the effect of diameter-to-height ratio
S-0.4	120	0.4	0	
S-0.5	150	0.5	0	
S-0.4-1C	120	0.4	1	Analyzing the effects of circumferential CFRP wrap around holes and the number of wrap layers
S-0.4-2C	120	0.4	2	

Note: The diameter-to-height ratio refers to the ratio of the circular hole diameter to the beam height.

2.3. Test setup, measurements and loading procedure

The four-point bending tests on the timber beams were conducted. The loading setup and sensor arrangement are illustrated in Figure 2. A preloading step was first applied to the timber beams. After confirming the proper functioning of the instrumentation, the beams were unloaded to their original state. Formal loading was performed using a displacement-controlled mode, with an initial loading rate of 2 mm/min. When cracking occurred in the timber beams, the loading rate was reduced to 1.5 mm/min until complete failure of the specimens. To measure the vertical deformation of the timber beams during loading, five displacement transducers were arranged at the loading points, supports, and mid-span of the specimen. To measure the principal strain around the hole, four strain gauges (labeled C1 to C4) were arranged counterclockwise along the edge of the hole. All load, displacement, and strain data were measured and recorded using the TDS 530 data acquisition system. The Digital Image Correlation Method (DICM) was employed to quantitatively analyze the vertical strain field around the openings.

Fig. 2: Layout of test loading device and measuring points (unit: mm): (a) actual photograph; (b) schematic diagram.

3. Test results and discussion

3.1. Failure modes

The failure morphology of the non-perforated beam specimen S-0 is shown in Figure 3. During the initial loading stage, faint acoustic emissions were detected from the timber, and minor cracks formed at defects in the tension zone, such as knots, slope of grain, and mechanical joints. As the load increased, the tension zone edge reached its ultimate tensile strain, causing cracks to propagate rapidly upward in a zigzag pattern. At failure, extensive bending cracks appeared at the mid-span of Specimen S-0, while the top compression zone exhibited no buckling deformation, demonstrating a typical brittle tensile failure under bending. This behavior arises because natural and manufacturing defects in the timber disrupted the integrity

and continuity of the longitudinally aligned tensile fibers. These defects induced localized stress concentrations in the tension zone, accelerating the attainment of the ultimate tensile strain and triggering sudden failure.

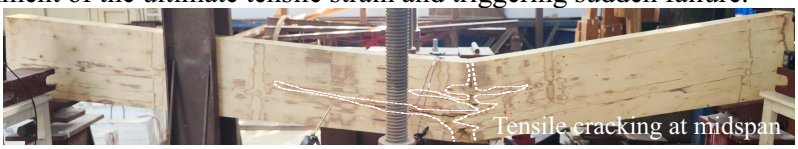

Fig. 3: Failure mode of specimen S-0.

Figure 4 shows the failure mode of specimen S-0.3. All unreinforced beams with a hole displayed similar shear failure characteristics. The following description uses specimen S-0.3 as a detailed example. During the initial loading stage, a crack developed in the upper-right section of the inner wall of the circular hole (at an angle of approximately 45° to the beam's longitudinal axis) in the mid-width position due to stress concentration (Figure 4a). Subsequently, a new crack began to form in the lower-left section of the inner wall of the circular hole (at an angle of about 225°) in the mid-width position (Figure 4b). As the load and deformation increased, these cracks rapidly spread across the width of the section to the area around the hole (Figure 4c), and quickly extended along the grain toward the support and loading ends. Ultimately, when the crack in the lower left side around the hole reached the support end, the beam experienced shear displacement due to inconsistent deformation above and below the crack, causing the timber beam to fail. This type of failure exhibited a typical shear failure along the grain (Figure 4d).

Fig. 4: Failure mode of specimen S-0.3: (a) cracking in the upper-right section; (b) cracking in the lower-left section; (c) cracks extending to the hole's periphery; (d) global failure mode.

The failure modes observed in specimen S-0.3 indicate that the failure of unreinforced beams with a hole is primarily caused by the formation and propagation of cracks around the hole. The hole presence not only leads to plastic deformation around the hole, reducing the mechanical properties of LVL, but also decreases the effective cross-sectional area, resulting in stress concentration. Consequently, cracks tend to form at locations with the highest perpendicular-to-grain tensile strain, typically at angles of about 45° or 225° to the beam's longitudinal axis. Given LVL's high anisotropy and relatively low perpendicular-to-grain tensile strength, these cracks extend along the grain, forming perpendicular-to-grain tension cracks. The presence of tension cracks results in a reduction of the effective shear area within the plane where they occur, an increase in longitudinal shear deformation under external loads, inconsistent deformation above and below the crack, and stress concentration at the crack tips. Consequently, this decreases the shear capacity of beams with holes.

Figure 5 shows the failure mode of specimen S-0.4-2C. The failure modes of specimens S-0.4-1C and S-0.4-2C are similar, with both exhibiting shear failure. Although the crack in the lower-left inner wall of the hole formed earlier than the crack in the upper-right inner wall (Figures 5a and 5b), the failure mechanism of CFRP-reinforced beams with a hole is still like that of unreinforced beams. Notably, the circumferential CFRP wrap had little impact on the initial crack angle for specimen S-0.4-2C, which remained approximately 45° or 225° (Figure 5c). Tension cracks in the perpendicular-to-grain direction split the beam into upper and lower layers (Figure 5d), while the circumferential CFRP wrap around the hole underwent shear deformation due to the applied shear force (Figure 5e). The ultimate along-the-grain shear crack extended from the lower-left of the hole to the support end. Despite the inability to prevent crack formation, circumferential CFRP wrap significantly limited crack propagation. Compared to specimen S-0.4-2C, specimen S-0.4-1C exhibited greater shear displacement at the beam-ends during failure (Figure 5f), indicating a lower level of shear reinforcement. In comparison to unreinforced beams with a hole, CFRP-reinforced beams with a hole displayed less severe perpendicular-to-grain tension

cracking and greater ductility at ultimate failure. This improved performance is mainly due to circumferential CFRP wrap reducing stress concentration at the crack tips and their restraining effect limiting crack propagation.

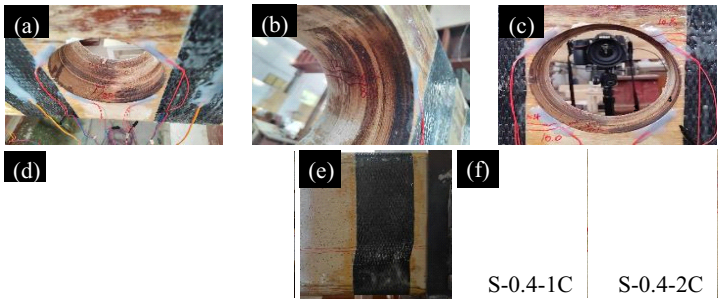

Fig. 5: Failure mode of specimen S-0.4-2C: (a) cracking in the lower-left section; (b) cracking in the upper-right section; (c) cracks extending to the hole's periphery; (d) crack extending along the grain; (e) shear deformation of circumferential CFRP wrap; (f) shear displacement at the beam-end.

3.2. Load-deflection curves

Figure 6 shows the load-deflection (F-δ) curves for all specimens, while Table 3 provides the experimental results for each specimen. Where, F_{cr} refers to the cracking load, representing the load on poplar LVL beams when the first major crack appears at the upper-right or lower-left edge of the hole. F_u is the ultimate load at which the poplar LVL beam fails. δ_{cr} and δ_u are the deflection at midspan when cracking occurs and the ultimate deflection at failure, respectively.

Fig. 6: Load-deflection curves: (a) effect of diameter-to-depth ratio; (b) effect of the number of layers of circumferential CFRP wrap.

Table 3: Characteristic load, deflection and failure modes.

No.	F_{cr}/kN	δ_{cr}/mm	F_u/kN	δ_u/mm	Crack initiation location	Final failure location	Failure mode
S-0	/	/	149.21	48.94	Mid-span	Mid-span	Bending failure
S-0.3	96.14	26.78	122.45	37.19	Upper-right of the hole	Beam-end	Shear failure
S-0.4	80.21	21.98	100.12	29.41	Upper-right of the hole	Beam-end	Shear failure
S-0.5	72.49	19.47	89.02	24.87	Upper-right of the hole	Beam-end	Shear failure
S-0.4-1C	80.33	21.32	122.56	37.39	Lower-left of the hole	Beam-end	Shear failure
S-0.4-2C	83.16	21.49	141.41	48.64	Lower-left of the hole	Beam-end	Shear failure

As shown in Figure 6 and Table 3, prior to reaching the ultimate load, all specimens exhibited load-deflection curves without distinct yield points, demonstrating typical brittle failure characteristics. The load-deflection curve of the non-perforated beam specimen S-0 displayed the most pronounced nonlinearity, along with the highest ultimate load and deflection. As the diameter-to-height ratio increased, the ultimate load and deflection of perforated beam specimens S-0.3, S-0.4, and S-0.5 decreased sequentially. This is attributed to the fact that openings in the bending-shear region promote longitudinal cracks parallel to the beam axis, leading to stress concentration at crack tips and reduced deformation compatibility in the adjacent wood, thereby diminishing the load-bearing capacity and deflection of unreinforced perforated specimens. Compared to the non-perforated control specimen S-0, the ultimate loads of specimens S-0.3, S-0.4, and S-0.5

decreased by 17.9%, 32.9%, and 40.9%, respectively, with corresponding reductions in ultimate deflection of 23.0%, 39.1%, and 48.8%. Furthermore, the failure modes of specimens S-0.3, S-0.4, and S-0.5 shifted to longitudinal shear failure at the beam ends. When the diameter-to-depth ratio increased from 0.3 to 0.4 and 0.5, the ratio of cracking load to ultimate load for perforated beams rose from 0.79 to 0.80 and 0.81, respectively. These results indicate that openings in the bending-shear region alter the failure mode of timber beams, with the diameter-to-depth ratio being a critical factor governing their mechanical performance. As the diameter-to-height ratio increases, perforated beams exhibit more pronounced brittle characteristics during shear failure.

After reinforcement with circumferential CFRP fabric, the load-deflection curves of the perforated beams exhibited pronounced nonlinearity. Compared to the non-perforated control specimen S-0, the ultimate loads of the reinforced perforated beam specimens S-0.4-1C and S-0.4-2C decreased by only 17.9% and 5.22%, respectively, with corresponding reductions in ultimate deflection of 22.6% and 0.62%. This indicates that the ultimate load and deflection of the CFRP-reinforced perforated poplar LVL beam specimens were nearly restored to the levels of the non-perforated timber beams. The improvement is attributed to the CFRP hoops enhancing shear performance by participating in shear resistance, redistributing shear stresses around the openings, and mitigating stress concentration at crack tips. Furthermore, the use of two layers of CFRP fabric around the openings more effectively compensated for the adverse effects of perforations, allowing the timber to better utilize its inherent mechanical properties. However, compared to the unreinforced perforated specimen S-0.4, the CFRP-reinforced specimens S-0.4-1C and S-0.4-2C showed no significant improvement in cracking load or cracking deflection, with variations of less than 5%. This is because cracks corresponding to the cracking load typically initiate at the mid-width of the opening walls. While CFRP reinforcement can restrict crack propagation, it cannot prevent crack initiation at this stage.

3.3. Load- principal strain curves

Figure 7 presents the load- principal strain (F-ε_p) curves for all specimens. Where the rectangular region around the hole is divided into four quadrants (quadrants I ~ IV). The experimental results show that the principal tensile strains around the hole are primarily distributed in quadrants I and III, while the principal compressive strains are concentrated in quadrants II and IV. This aligns with the observed test results, where the hole's shape changes from circular in the unloaded state to elliptical at final failure. For specimens S-0.3, S-0.4, and S-0.5, the load-hole's periphery principal strain relationship appears approximately linear, with a reduction in the slope as the diameter-to-height ratio increases. This reduction is mainly due to the stress concentration around the hole, which weakens the poplar LVL's stiffness. After circumferential CFRP wrap around the hole, the load-hole's periphery principal strain curves for specimens S-0.4-1C and S-0.4-2C exhibit some nonlinearity. This suggests that circumferential CFRP wrap contributes to shear resistance and helps distribute the stress at the ends of cracks, reducing the impact of stress concentration. The principal tensile and compressive strains around the hole in reinforced beam specimens are greater than those in unreinforced beam specimens, which is likely due to the greater deformation occurring in the reinforced beams during loading.

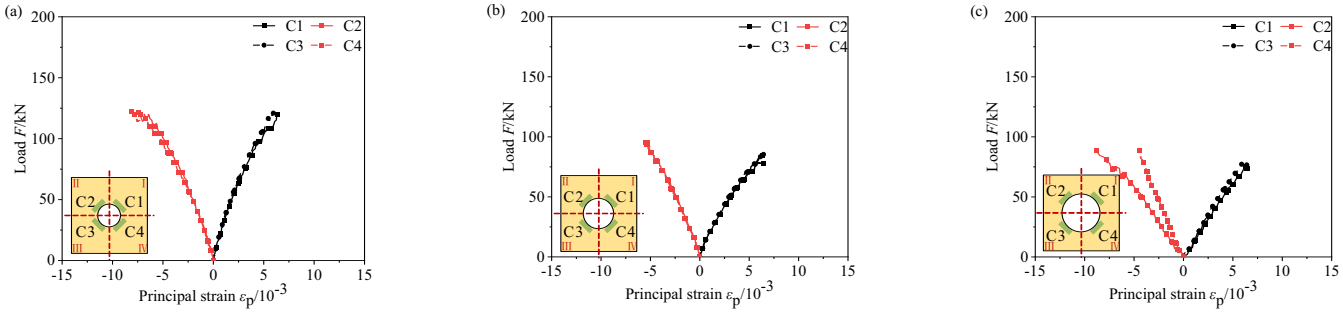

Fig. 7: Load- principal strains: (a) S-0.3; (b) S-0.4; (c) S-0.5; (d) S-0.4-1C; (e) S-0.4-2C.

3.4. Hole's periphery normal strain nephogram based on DICM

The normal strain contour plots for specimens S-0.3, S-0.4, S-0.5 and S-0.4-1C, are depicted in Figure 8. Where, $\varepsilon_{\perp x}$ represents the perpendicular-to-grain strain, with tensile strain being positive and compressive strain being negative. The experimental results showed that DICM can accurately and reliably evaluate the initial location of cracks and the corresponding strain components, and the strain distribution in the CFRP fabric can reflect the propagation of cracks. The perpendicular-to-grain tensile strain around the hole mainly occurs in quadrants I and III, while the perpendicular-to-grain compressive strain primarily occurs in quadrants II and IV. The maximum perpendicular-to-grain tensile strain around the hole forms an angle of approximately 45° or 225° with respect to the longitudinal axis of the beam, consistent with the initial cracking angle around the hole. As the diameter-to-height ratio increases, the concentration of perpendicular-to-grain tensile strain around the hole also increases for specimens S-0.3, S-0.4, and S-0.5. Specimen S-0.4-1C has the smallest concentrated region of perpendicular-to-grain tensile strain, indicating that circumferential CFRP wrap helps to resist shear and alleviate stress concentration at the crack tips, thereby also limiting crack propagation.

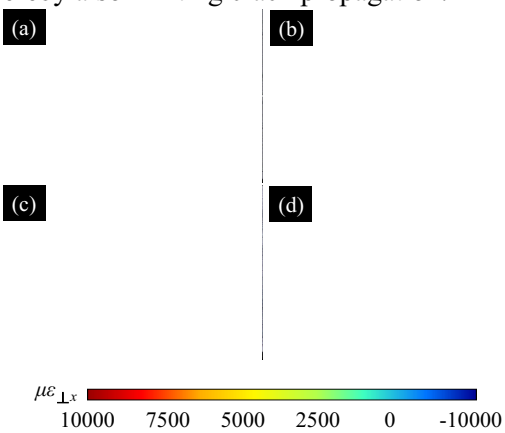

Fig. 8: Normal strain contour plots of hole-periphery: (a) S-0.3; (b) S-0.4; (c) S-0.5; (d) S-0.4-1C.

4. Conclusion

(1) The failure mode of the unperforated LVL beams was tensile failure due to mid-span bending, while the failure mode of the perforated beams was longitudinal shear failure at the beam ends. The maximum transverse tensile strain around the openings formed angles of approximately 45° or 225° with the longitudinal axis of the beam, consistent with the crack initiation angles at the openings. The transverse tensile strains around the openings were primarily distributed in Quadrants I and III, whereas the transverse compressive strains were concentrated in quadrants II and IV.

(2) When the diameter-to-height ratio was 0.4, the ultimate load of perforated beams with 1 and 2 layers of circumferential CFRP fabric decreased by only 17.9% and 5.22%, respectively, compared to unperforated beams. The application of CFRP fabric wrapping around the openings effectively inhibited crack propagation and improved the mechanical performance of the perforated beams.

(3) Under the same opening location, as the diameter-to-height ratio increases to 0.5, both the cracking load and ultimate load of the perforated beams decrease significantly. When the diameter-to-height ratio rises from 0.3 to 0.4 and 0.5, the ratio

of cracking load to ultimate load increases from 0.79 to 0.80 and 0.81, respectively, exhibiting more pronounced brittle characteristics during shear failure.

Acknowledgements

The authors would like to acknowledge the financial support to the work by the National Natural Science Foundation of China (CN 51878590), Yangzhou University Graduate International Academic Exchange Special Fund Project (YZUF2024110) and International Academic Exchange Fund for Doctoral Students of Yangzhou University (2025).

References

[1] W. Long, Wood structure design manual, 4th ed. Beijing: China Architecture & Building Press, 2005. (in Chinese)
[2] K. Yue, "The study on mechanical properties and durability of modified fast-growing poplar wood," M.S. thesis, Nanjing Forestry Univ., Nanjing, China, 2008, p. 2. (in Chinese)
[3] J. Y. Tang, X. B. Song, Y. Guo, Y. K. Song, "Residual strain and elastic-plastic damage of wood due to hole drilling," J. Build. Struct., vol. 44, no. 10, pp. 114-122, 2023. (in Chinese)
[4] G. Chen, H. T. Li, T. Zhou, C. L. Li, Y. Q. Song, R. Xu, "Experimental evaluation on mechanical performance of OSB webbed parallel strand bamboo I-joist with holes in the web," Constr. Build. Mater., vol. 101, pp. 91-98, 2015.
[5] M. Ardalany, M. Fragiacomo, D. Carradine, P. Moss, "Experimental behavior of laminated veneer lumber (LVL) joists with holes and different methods of reinforcement," Eng. Struct., vol. 56, pp. 2154-2164, 2013.
[6] E. C. Zhu, Z. W. Guan, P. D. Rodd, D. J. Pope, "Finite element modelling of OSB webbed timber I-beams with interactions between openings," Adv. Eng. Softw., vol. 36, no. 11/12, pp. 797-805, 2005.
[7] Y. Wei, S. Chen, S. Tang, D. Peng, K. Zhao, "Mechanical response of timber beams strengthened with variable amounts of CFRP and bamboo scrimber layers," J. Compos. Constr., vol. 26, no. 4, pp. 04022038, 2022.
[8] T. Gentry, "Performance of glued-laminated timbers with FRP shear and flexural reinforcement," J. Compos. Constr., vol. 15, no. 5, pp. 861-870, 2011.
[9] Z. B. Ling, W. Q. Liu, J. S. Shao, "Experimental and theoretical investigation on shear behaviour of small-scale timber beams strengthened with fiber-reinforced polymer composites," Composite Structures, vol. 240, pp. 111989, 2020.
[10] Y. L. Yang, J. W. Liu, G. J. Xiong, "Flexural behaviour of wood beams strengthened with HFRP," Constr. Build. Mater., vol. 43, pp. 118-124, 2013.
[11] Y. Pan, R. B. An, C. T. Zhang, Y. X. Wang, "Experimental study on flexural behavior of BFRP reinforced circular timber beams," J. Build. Struct., vol. 40, no. 10, pp. 197-206, 2019. (in Chinese)